ACS Infectious Diseases

pubs.acs.org/journal/aidcbc Article

Quinoline and Quinazoline Derivatives Inhibit Viral RNA Synthesis by SARS-CoV-2 RdRp

Jianyuan Zhao,[⊥] Yongxin Zhang,[⊥] Minghua Wang,[⊥] Qian Liu,[⊥] Xiaobo Lei, Meng Wu, SaiSai Guo, Dongrong Yi, Quanjie Li, Ling Ma, Zhenlong Liu, Fei Guo, Jianwei Wang, Xiaoyu Li,* Yucheng Wang,* and Shan Cen*

Cite This: *ACS Infect. Dis.* 2021, 7, 1535−1544 Read Online

ACCESS | Metrics & More | Article Recommendations | Supporting Information

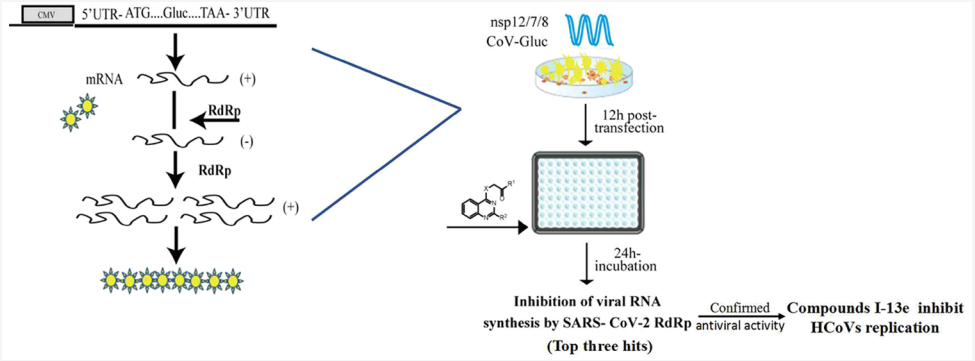

ABSTRACT: Coronavirus disease 2019 (COVID-19) is a fatal respiratory illness caused by severe acute respiratory syndrome coronavirus 2 (SARS-CoV-2). The identification of potential drugs is urgently needed to control the pandemic. RNA dependent RNA polymerase (RdRp) is a conserved protein within RNA viruses and plays a crucial role in the viral life cycle, thus making it an attractive target for development of antiviral drugs. In this study, 101 quinoline and quinazoline derivatives were screened against SARS-CoV-2 RdRp using a cell-based assay. Three compounds **I-13e**, **I-13h**, and **I-13i** exhibit remarkable potency in inhibiting RNA synthesis driven by SARS-CoV-2 RdRp and relatively low cytotoxicity. Among these three compounds, **I-13e** showed the strongest inhibition upon RNA synthesis driven by SARS-CoV-2 RdRp, the resistance to viral exoribonuclease activity and the inhibitory effect on the replication of CoV, thus holding potential of being drug candidate for treatment of SARS-CoV-2.

KEYWORDS: *COVID-19, SARS-CoV-2, Quinoline and quinazoline derivatives, RdRp inhibitors*

Coronavirus disease 2019 (COVID-19) is a fatal respiratory illness caused by the severe acute respiratory syndrome coronavirus 2 (SARS-CoV-2).[1] Infected people usually showed signs of diseases including fever, fatigue, dry cough, as well as some less common symptoms such as headache, hemoptysis, and diarrhea within 14 days.[2] Most of the patients may finally develop dyspnoea and pneumonia and, in some severe cases, may have respiratory failure, septic shock, and/or multiple organ failure.[3] COVID-19 has been raised as a global public health crisis with more than 140.3 million confirmed cases, including over 3.0 million deaths having occurred worldwide by April 18, 2021.[4] The identification of potential drugs is therefore urgently needed to control the pandemic.

SARS-CoV-2 is a positive-sense single-stranded RNA virus belonging to the Betacoronavirus genus.[5,6] The SARS-CoV-2 genome comprises about 30 000 nucleotides in the order of 5′-replicase-S-E-M-N-3′.[7] The replicase gene is the only protein translated from the genome, and the products of other downstream genes are derived from subgenomic mRNAs. The replicase gene encodes two overlapping polyproteins (pp1a and pp1ab), which encode 16 nonstructural proteins (nsp1 to nsp16) for viral replication and transcription.[8,9] Among these nonstructural proteins, nsp12 serves as the RNA-dependent RNA polymerase (RdRp) which catalyzes the viral genome replication and transcription. Further studies have shown that viral RNA synthesis also requires two other factors, nsp7 and nsp8, which are proposed to have primase or 3′-terminal adenylyl-transferase activity.[10,11] RdRp is a conserved protein within RNA viruses, and it plays a crucial role in the viral life

Special Issue: Antiviral Therapeutics

Received: February 17, 2021
Published: May 26, 2021

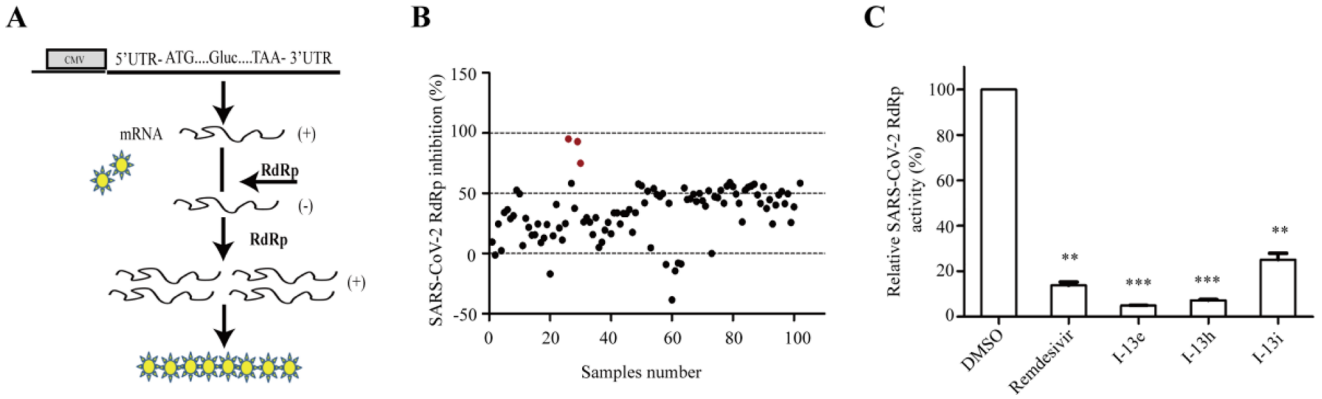

Figure 1. Identification of **I-13e**, **I-13h**, and **I-13i** as SARS-CoV-2 RdRp inhibitors. (A) Schematic diagram of the Gluc reporter system. The expression cassette of Gluc is in the sense strand, which is flanked by the 5′ and 3′ untranslated regions (UTRs) of SARS-CoV-2. The negative-sense vRNA is first synthesized by SARS-CoV-2 RdRp (nsp12, nsp7, and nsp8), followed by transcription into plus-strand RNA (mRNA) to magnify the Gluc signal. (B, C) Screening result of the 101 quinoline and quinazoline derivatives. The red spots represent compounds **I-13e**, **I-13h**, and **I-13i** for which inhibitory activity > 70%. Results shown are the average of three independent experiments. Error bars indicate SD, $^{**}p < 0.01$, $^{***}P < 0.001$.

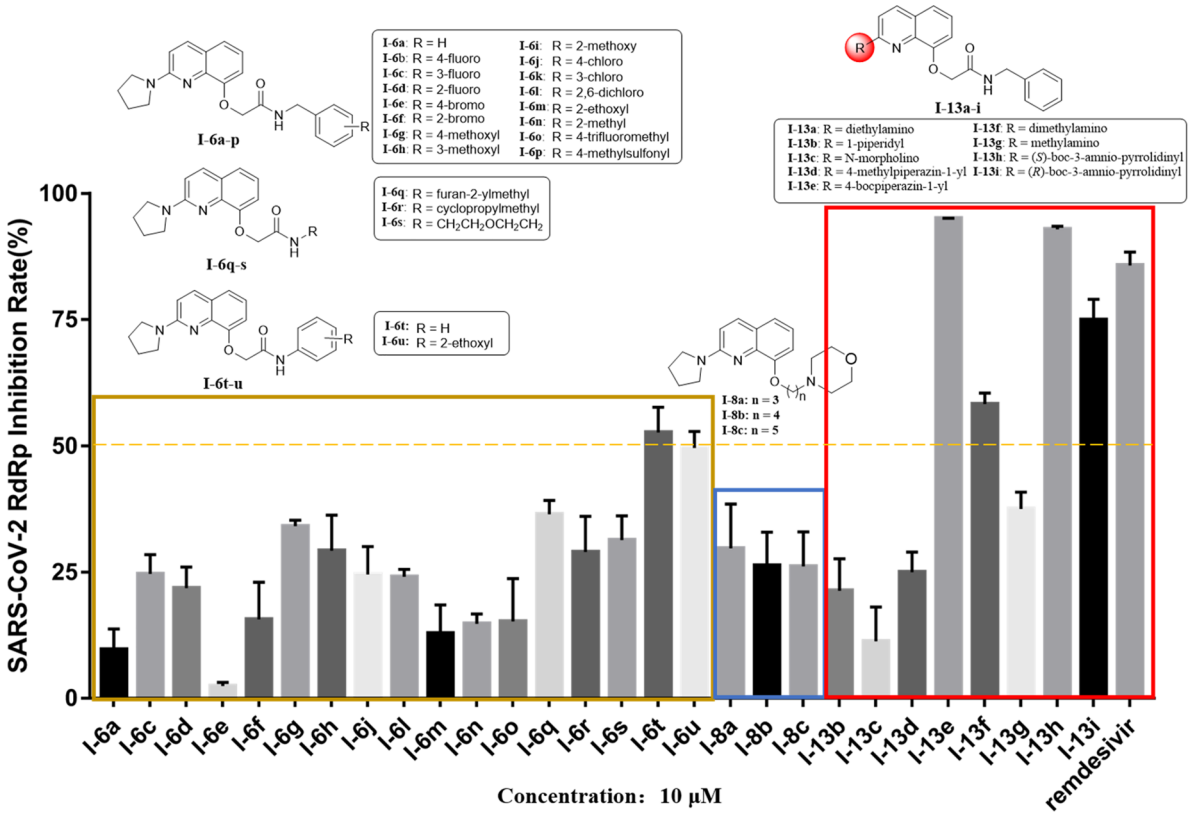

Figure 2. Inhibition rate of the quinoline derivatives against SARS-CoV-2 RdRp. HEK293T cells were transfected with CoV-Gluc, nsp12, nsp7, and nsp8 plasmid at a ratio of 1:10:30:30. Cells were reseeded in 96-well plates (10^4/well) 12 h post transfection and then treated with the indicated compounds at the concentration of 10 μM. After 24 h incubation, Gluc activity in supernatants was determined. Inhibition values are shown. Results shown are the average of three independent experiment and error bars indicate SD.

cycle, thus making it an attractive target for development of antiviral drugs.[12]

Quinoline and quinazoline derivatives are belonging to an important class of heterocyclic compounds, which have a wide range of biological properties such as antibacterial,[13] antifungal,[14,15] ant-cancer[16] and antiviral activities.[17−19] Interestingly, quinoline and quinazoline derivatives not only inhibit RNA viruses such as HIV-1,[20] Ebola Virus (EBOV),[21] Respiratory Syncytial Virus (RSV),[22] hepatitis C virus (HCV),[22] and influenza A virus (IAV)[23,24] but also exhibit activities against DNA virus such as herpes simplex virus (HSV)[25] and hepatitis B virus (HBV).[26] Nevertheless, several studies and our previous work indicated that the activities of quinazoline derivatives against RNA virus are mainly derived from their inhibitory activity upon the RNA synthesis driven by the RdRp of these viruses.[18,22,23] Given the structural similarity of core domain within RdRp, it raises a possibility that quinoline and quinazoline derivatives may also target the

https://doi.org/10.1021/acsinfecdis.1c00083
ACS Infect. Dis. 2021, 7, 1535−1544

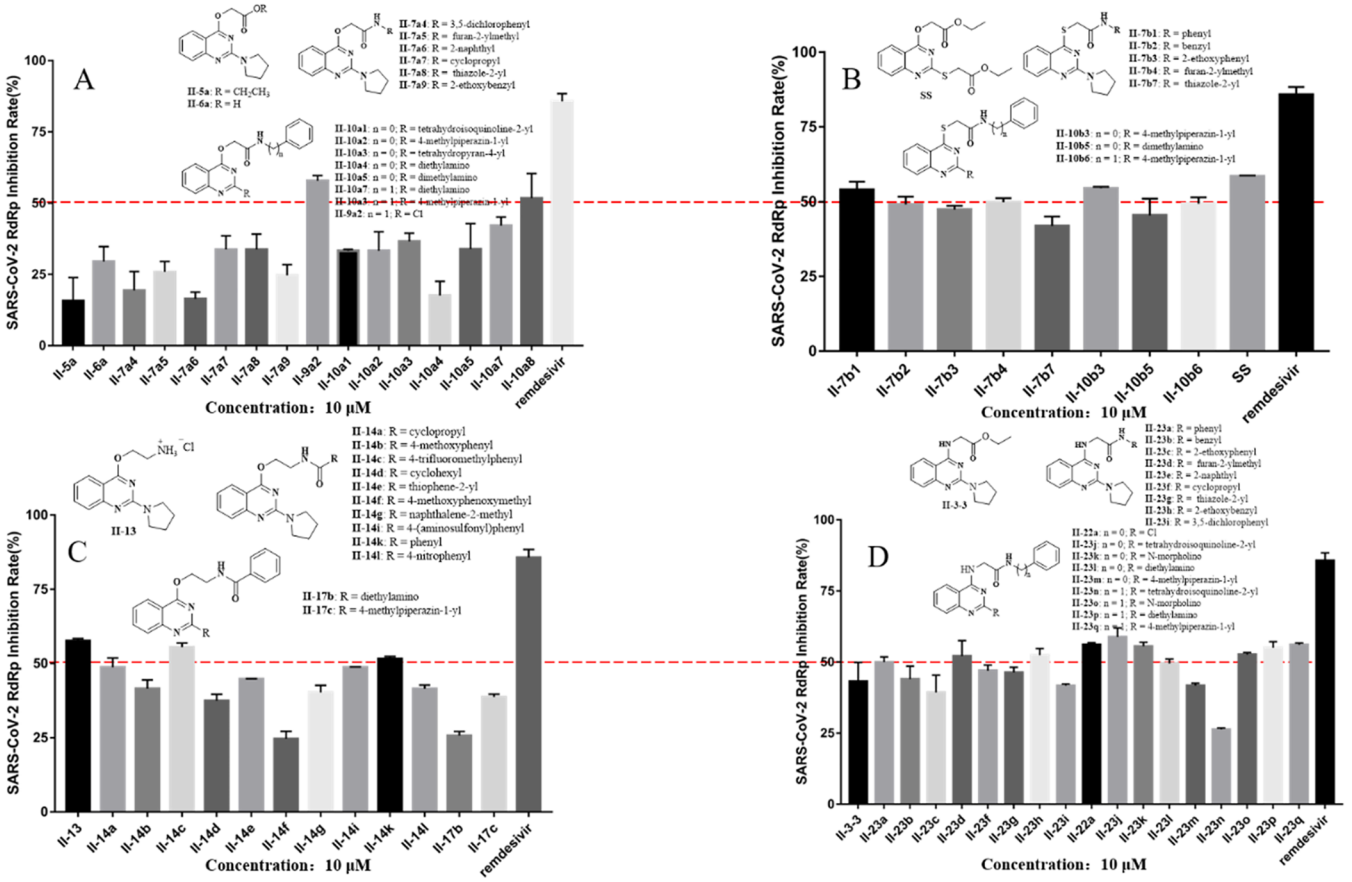

Figure 3. Inhibition rate of the quinazoline derivatives against SARS-CoV-2 RdRp. HEK293T cells were transfected with CoV-Gluc, nsp12, nsp7, and nsp8 plasmid at a ratio of 1:10:30:30. Cells were reseeded in 96-well plates (10^4/well) 12 h post transfection, and then treated with the indicated compounds above at the concentration of 10 μM. After 24 h incubation, Gluc activity in supernatants was determined and inhibition value is shown in Figure 3. Results shown are the average of three independent experiment and error bars indicate SD.

RdRp of SARS-CoV-2. Because no data have been reported so far, we therefore evaluated a series of quinoline and quinazoline derivatives for their antiviral activities against SARS-CoV-2 using our previously developed cell-based SARS-CoV-2 RdRp report system, aiming at finding a new class of anti-SARS-CoV-2 drug candidates.

RESULT

Inhibition of SARS-CoV-2 RdRp by Quinoline Derivatives. In the previous study, we developed a cell-based SARS-CoV-2 RdRp report system which can be deployed to discover SARS-CoV-2 RdRp inhibitors.[27] The system was composed of two parts: a Gluc reporter plasmid and the plasmids for expressing SARS-CoV-2 RdRp which is basically composed of nsp7, nsp8, and nsp12. The Gluc gene was under a tetracycline regulated expression promoter and flanked by 5′ and 3′ untranslated regions (UTRs) of SARS-CoV-2. When trace amounts of Gluc mRNA are transcripted, the UTRs flanking the mRNA can be recognized by the SARS-CoV-2 RdRp and then the Gluc mRNA is amplified by viral RdRp, resulting in the substantial increase of Gluc expression (Figure 1A). Therefore, the increased Gluc activity reports the activity of SARS-CoV-2 RdRp.

Using this assay, we analyzed a serial of quinoline and quinazoline derivatives that were previously reported to have significant activity against the RdRp of the influenza A virus. Among all the 101 compounds that we tested, 22 compounds showed inhibition activity over 50% at 10 μM (Figure 1B and Table S1). Among them, three quinoline derivatives (**I-13e**, **I-13h**, and **I-13i**) showed the most potent inhibition ratio (95.03%, 92.85%, 74.94%, respectively) (Figure 1C). Furthermore, we have assessed the effect of the active compounds **I-13e**, **I-13h**, and **I-13i** on the mRNA transcription from the Gluc reporter plasmid in the absence of viral RdRp. Briefly, HEK293T cells were cotransfected with a pCoV-Gluc plasmid and incubated with **I-13e**, **I-13h**, and **I-13i**, respectively. Then levels of Gluc mRNA were determined by real-time RT-PCR. The main findings are presented in Figure S1 and show that these compounds have no significant impact on the level of Gluc mRNA in the absence of SARS-CoV-2 RdRp even at a higher concentration of 10 μM. This suggests that these compounds target the replication of RNA driven by viral RdRp.

The inhibition rate of the quinoline and quinazoline derivatives against SARS-CoV-2 RdRp along with remdesivir for comparison are summarized in Figure 2 and Table S1. The introduction of substituents on benzyl at the 8-position of the quinoline ring had a certain improvement of the activity compared with **I-6a**, such as F (**I-6c**, **I-6d**), Cl (**I-6j**, **I-6l**), methoxyl (**I-6g**, **I-6h**), ethyoxyl (**I-6m**), and trifluoromethyl (**I-6o**). Among them, 4-OCH_3 contributed the most to the activity. However, the introduction of Br (**I-6e**) markedly reduced the activity. Replacing the benzyl (**I-6a**) with furan-2-ylmethyl (**I-6q**), cyclopropylmethy (**I-6r**), or phenyl (**I-6t**)

https://doi.org/10.1021/acsinfecdis.1c00083
ACS Infect. Dis. 2021, 7, 1535−1544

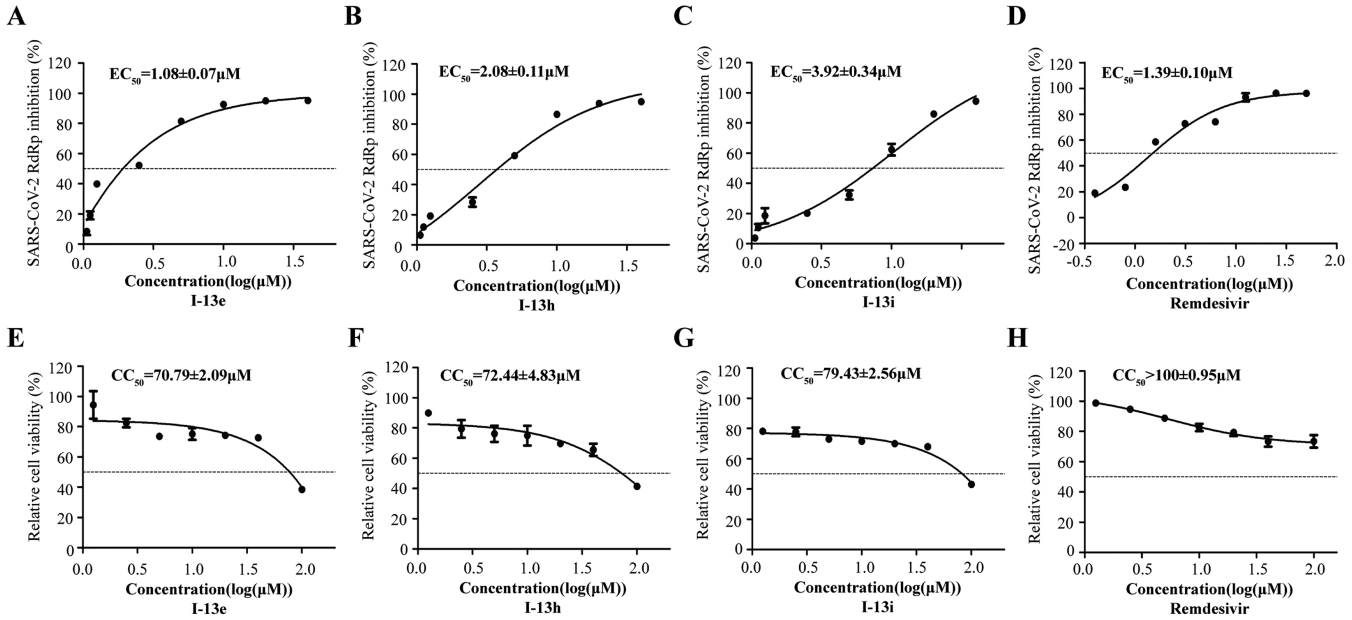

Figure 4. Dose−response curves (EC_{50} and CC_{50}) for the top three compounds. HEK293T cells were transfected with CoV-Gluc, nsp12, nsp7, and nsp8 plasmid at a ratio of 1:10:30:30. Cells were reseeded in 96-well plates (10^4/well) 12 h post transfection and then treated with serially diluted **I-13e**, **I-13h**, **I-13i**, and remdesivir. After 24 h incubation, Gluc activity in supernatants was determined and EC_{50} value was shown in (A-D). To assess cell viability, HEK293T cells (10^4/wells) were seeded in 96-well plates, and treated with these inhibitors as indicated above. The CC_{50} values were measured with CCK-8 Kit as shown in (E−H). Results shown are the average of three independent experiment and error bars indicate SD.

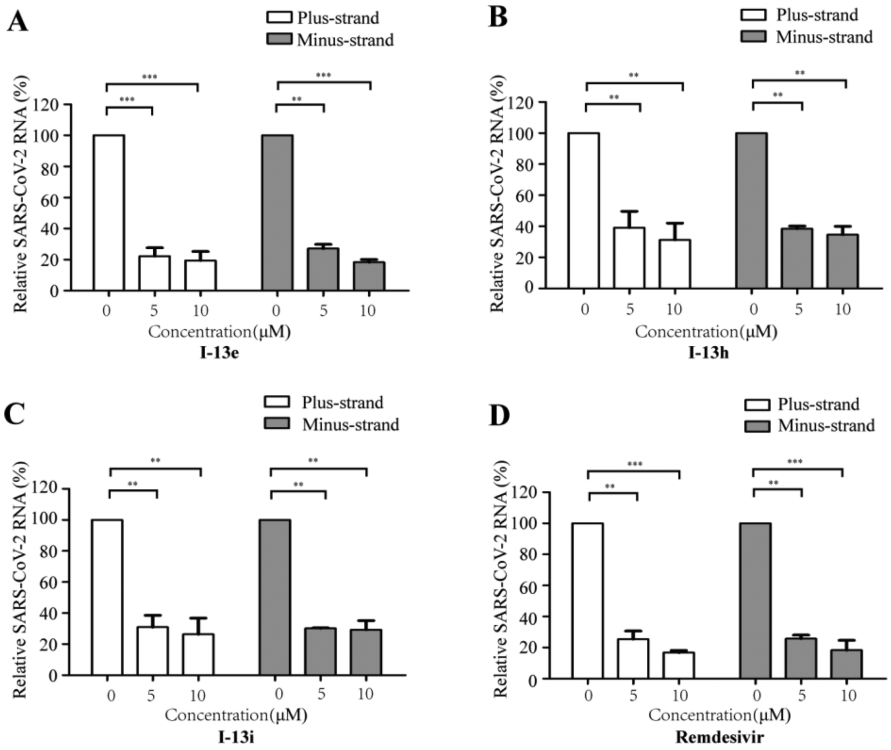

Figure 5. Inhibition of CoV-Gluc RNA expression by **I-13e**, **I-13h**, and **I-13i**. HEK293T cells were transfected with CoV-Gluc, nsp12, nsp7, and nsp8 plasmid DNA at a ratio of 1:10:30:30. Six hours post transfection, supernatants were replaced with fresh medium containing I-13e(A), I-13h(B), I-13i(C) and Remdesivir (D) respectively. Cells were cultured for 24 more hours, total cellular RNA was extracted, and levels of CoV-Gluc RNA were determined by real-time qRT-PCR. Results shown are the average of three independent experiments. Error bars indicate SD, $^{**}p < 0.01$, $^{***}P < 0.001$.

enhanced the activity against SARS-CoV-2 RdRp, while compounds with phenyl (**I-6t**) and 2-ethoxyl phenyl (**I-6u**) showed relatively higher activity. When the acyl chain at the 8-position was replaced by the corresponding ether chain (**I-8a**−**c**), equivalent activity was observed compared with **I-6s** and an increase of some activity was observed compared with **I-6a**, indicating that its carbonyl group may not be necessary. Otherwise, the carbonyl group could be involved in the

https://doi.org/10.1021/acsinfecdis.1c00083
ACS Infect. Dis. 2021, 7, 1535−1544

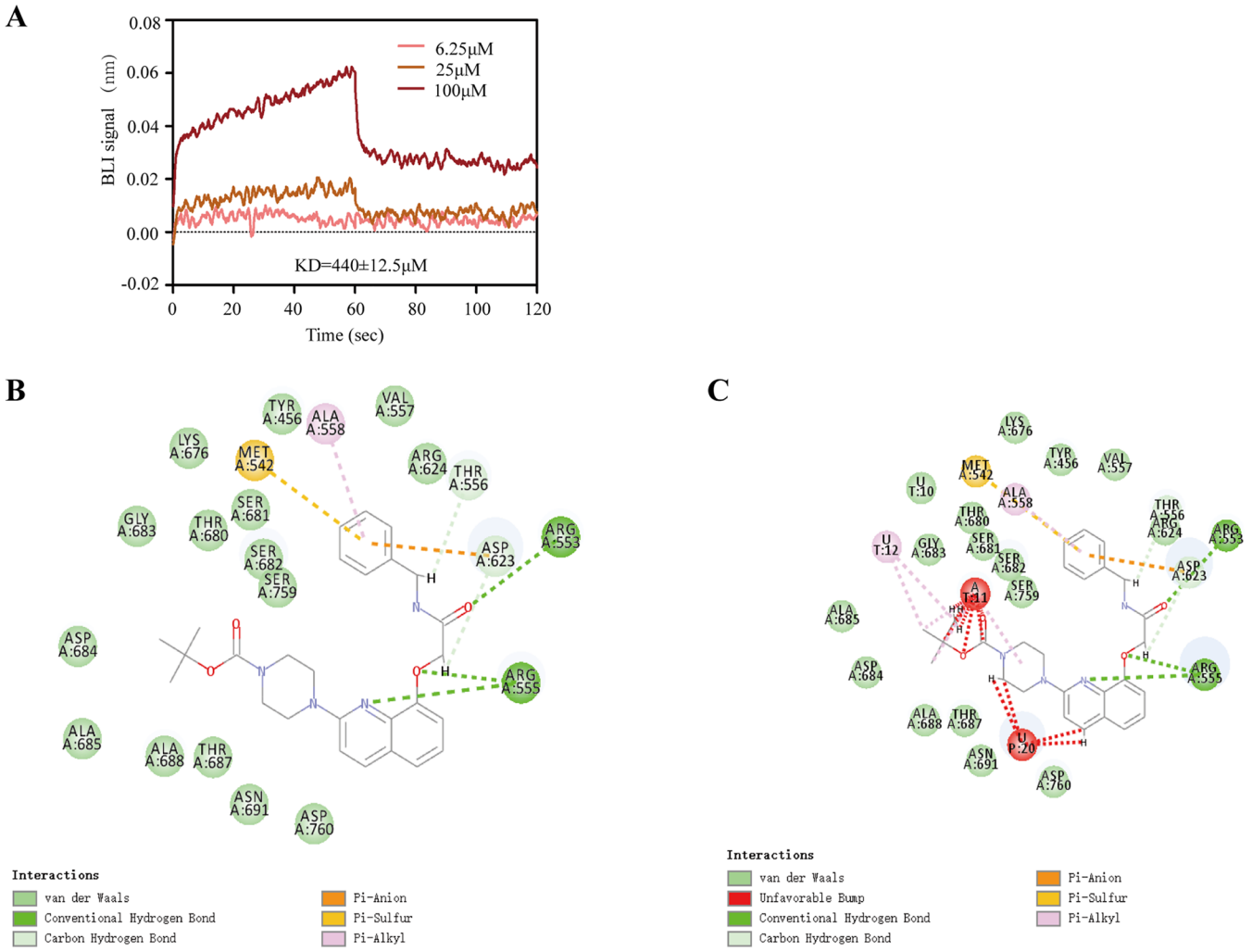

Figure 6. Kinetic and equilibrium binding analysis of peptides binding to SARS-CoV-2 RdRp and predicted binding site of **I-13e** in RdRp. (A) Kinetic and equilibrium binding analysis of **I-13e** binding to nsp12. Purified nsp12 (50 μg/mL) was captured via Ni-NTA biosensors and then dipped into 6.25, 25, and 100 μM **I-13e**, respectively. The association and dissociation curves of the compound are shown. K_D values were acquired from fitting into a 1:1 binding model by global fitting of multiple kinetic traces and then analyzed by Data Analysis 9.0 software. Data shown are representative of three independent experiments, and error bars indicate SD (B) Predicted binding mode of **I-13e** with nsp12 RdRp. (C) Predicted binding mode of **I-13e** with nsp12 RdRp−RNA complex.

formation of hydrogen bonds which was beneficial to the activity.

For the 2-position of quinoline ring, the replacement of the pyrrolidinyl group by other groups had a significant influence on the activity. The piperidyl (**I-13b**), morpholine (**I-13c**), and *N*-methylpiperazinyl (**I-13d**) groups contributed little to the activity, whereas the boc-piperazinyl (**I-13e**) and (*S*)-boc-3-amnio-pyrrolidinyl **I-13h** derivatives significantly increased the activity (95.03%, 92.85%, respectively). The (3*R*)-configured **I-13i** showed some decreased activity compared to (3*S*)-configured **I-13h**. We have assessed the stability of **I-13e** in DMEM at 37 °C for 24 h using HPLC-MS, which resembles a similar condition for the activity analysis. The HPLC-MS spectra show that the structure and content of the compound did not change (Figure S2). We also synthesized the corresponding deprotected compounds **I-13e**, **I-13h**, and **I-13i** and assessed their activity against SARS-CoV-2 RdRp. Surprisingly, the inhibition rates for **I-13e-deboc**, **I-13h-deboc**, and **I-13i-deboc** at the concentration of 10 μM are 12.90 ± 3.21%, 11.57 ± 4.28%, and 11.39 ± 5.14%, respectively (Table S1), indicating that introducing hydrophobic groups at C-2 was more favorable to the activity, which provided a guidance for the next modification.

We could observe that the inhibition rates of quinazoline derivatives were around 50% except for *O*-acetamides at C-4 (Figure 3A). The activity against SARS-CoV-2 RdRp of the quinazoline derivatives depends on both of the groups at the C-2 and C-4 positions. The relative contribution of the substituents at the C-4 position to activity is as follows: NH-acetamide groups > *S*-acetamide groups > *O*-ethylamine groups > *O*-acetamide groups. Quinazoline derivatives did not show clear structure−activity relationships, which need further exploration (Figure 3B−D).

Inhibitory Activity of I-13e, I-13h, and I-13i upon RNA Synthesis by SARS-CoV-2 RdRp. We next measured the 50% effect concentration (EC_{50}) value of the **I-13e**, **I-13h**, and **I-13i**, and remdesivir was used as a positive control. The three compounds **I-13e**, **I-13h**, and **I-13i** displayed remarkable potency in inhibiting RNA synthesis by SARS-CoV-2 RdRp with EC_{50} values of 1.08, 2.08, and 3.92 μM, respectively, similar to the EC_{50} value (1.39 μM) of remdesivir (Figure 4A−D). We further determined in vitro the 50% cytotoxic

https://doi.org/10.1021/acsinfecdis.1c00083
ACS Infect. Dis. 2021, 7, 1535−1544

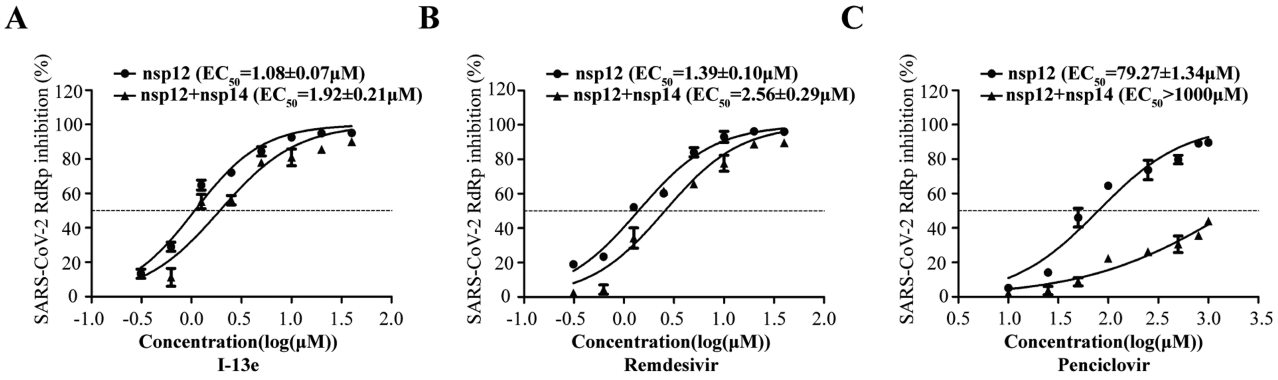

Figure 7. I-13e was resistant to the proofreading activity of nsp14/nsp10. HEK293T cells were co-transfected with CoV-Gluc, nsp12, nsp7, nsp8 with or without nsp10, and nsp14 plasmid at a ratio of 1:10:30:30:25:25. (A–C) EC_{50} values of **I-13e**, remdesivir, and penciclovir determined, respectively, by the cell-based system with the nsp10/nsp14 proofreading function. Results shown are the average of three independent experiment, and error bars indicate SD.

concentration (CC_{50}) for the defined therapeutic index (TI) (CC_{50}/EC_{50}). The CC_{50} value of the three compounds was 70.79, 72.44 and 79.43 μM, respectively (Figure 4E-H), with TI values of 65.55, 34.83, and 20.26, respectively. The compounds showed considerable inhibitory activity against RNA synthesis by SARS-CoV-2 RdRp and relatively low cytotoxicity.

I-13e, I-13h, and I-13i Inhibit SARS-CoV-2 Plus-Strand and Minus-Strand RNA Synthesis. We further examined the effect of the three compounds on the RNA synthesis efficiency of SARS-CoV-2 RdRp by quantifying the levels of plus-strand and minus-strand RNA of Gluc. The results showed that all three compounds as well as remdesivir can diminish the levels of both plus-strand RNA and minus-strand Gluc RNA in a dose-dependent manner. Remdesivir has 74% inhibition in both plus- and minus-strand RNA of Gluc at 5 μM concentration (Figure 5D), while **I-13e**, **I-13h**, and **I-13i** have 75%, 61% and 70% inhibition rates to both plus-strand RNA and minus-strand RNA of Gluc at the same concentration respectively (Figure 5A–C). These data further confirmed that **I-13e**, **I-13h**, and **I-13i** are inhibitors against RNA synthesis by SARS-CoV-2 RdRp.

I-13e Binds to the SARS-CoV-2 RdRp. To test if **I-13e**, **I-13h**, and **I-13i** inhibit SARS-CoV-2 RdRp activity by directly binding to it, we therefore tested whether **I-13e**, **I-13h**, and **I-13i** bind to SARS-CoV-2 RdRp by biolayer interferometry assay (BLI assay), which has been widely used to detect biomolecular interactions in real time. We first immobilized the purified nsp12 on the surface of the sensor chip and then passed through the compounds with different concentrations over the chip surface, thus detecting the association and dissociation curves of the compounds. Only **I-13e** revealed a binding affinity to nsp12 in a concentration-dependent manner, with a equilibrium dissociation constant (K_D) of 440 ± 12.5 μM (Figure 6A).

We further predicted the binding mode of **I-13e** with RdRp through molecular docking by using the CDOCKER module of Discovery Studio 3.5. The SARS-CoV-2 RdRp protein (PDB code: 7BV2) and **I-13e** were prepared by using Discovery Studio 3.5, and then **I-13e** was docked into the catalytic domain of nsp12 RdRp with or without RNA duplex appeared. The predicted binding mode of **I-13e** in the catalytic domain of RdRp is shown as Figure 6B. When binding to RdRp, **I-13e** formed three hydrogen bond interactions with ARG555 and ARG553 of RdRp. As ARG555 plays an important role in RNA–RdRp interaction,[28] we hypothesized that **I-13e** may interfere with RNA–RdRp interaction. This hypothesis was partially proved by the predicted binding mode of **I-13e** and the RNA–RdRp complex, which indicated that **I-13e** could form two unfavorable bumps with RNA in the RNA–RdRp complex (Figure 6C).

It should be noted that the calculated K_D value of **I-13e** to SARS-CoV-2 RdRp appears to be much higher than the measured EC_{50} value of **I-13e** in cells. This raises the possibility that the inhibition of **I-13e** on RNA synthesis may not mainly result from its direct binding to SARS-CoV-2 RdRp; the detailed mechanism awaits further investigation.

I-13e Was Resistant to Proofreading Activity of nsp14/nsp10. In the RdRp complex, exoribonuclease nsp14 and its activator nsp10 provide the proofreading function during coronavirus replication, which can excise erroneous mutagenic nucleotides incorporated by nsp12 into viral RNA, thus creating resistance to nucleotide analogue (NA) drugs.[22] Many NAs such as ribavirin can be excised from the growing RNA chain of CoVs, thus greatly affecting its antiviral activity.[29] Therefore, we need to explore whether the inhibition activity of **I-13e** is affected in the presence of nsp14 and nsp10. We expressed nsp14 and nsp10 in the cell-based CoV-RdRp-Gluc system. The Gluc activity slightly decreased in the presence of nsp14 and nsp10, which have been previously verified, compared to penciclovir, which was sensitive to proofreading activity against SARS-CoV-2 RdRp in the presence of nsp14 and nsp10, with an EC_{50} value of more than 1000 μM (Figure 7C). Remdesivir was proved resistant to proofreading activity provided by nsp14/nsp10, with an EC_{50} value of 2.56 μM (Figure 7B). **I-13e** also keeps its inhibitory activity against SARS-CoV-2 RdRp in the presence of nsp14 and nsp10, with an EC_{50} value of 1.92 μM (Figure 7A). These results demonstrate the insensitivity of **I-13e** to exoribonuclease activity, a great advantage over nucleotide analogues.

Evaluation of Antiviral Activity of I-13e against Human Coronavirus Strains HCoV-OC43 and HCoV-NL63. To assess if these compounds were effective against coronavirus replication, a cell-based assay was utilized using HCT-8 and LLC-MK2 cell lines infected with HCoV-OC43 and HCoV-NL63, respectively, which belong to betacoronaviruses and alphacoronaviruses, followed by measuring the protection of cell viability against CoV-induced cytopathic effect (CPE) as a readout. Using remdesivir as a positive control, we infected HCT-8 or LLC-MK2 cells with these two

https://doi.org/10.1021/acsinfecdis.1c00083
ACS Infect. Dis. 2021, 7, 1535–1544

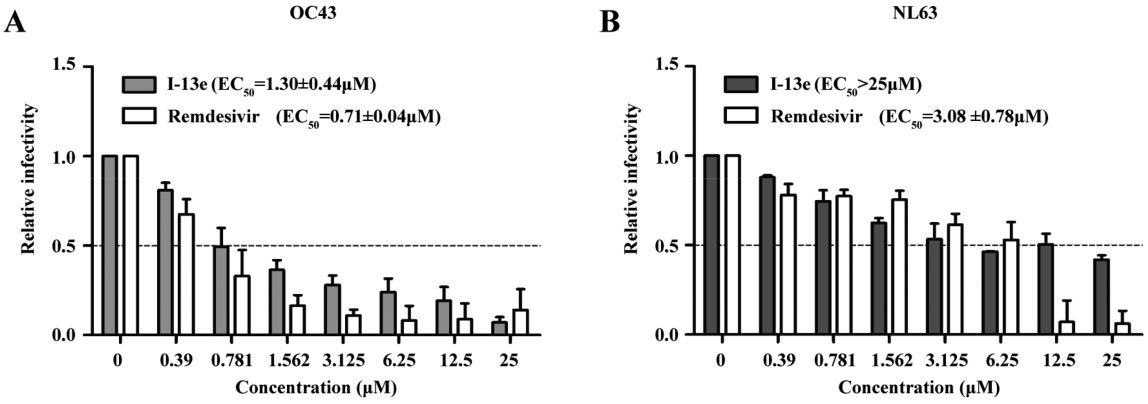

Figure 8. Evaluation of antiviral activity of **I-13e** against human coronavirus strains HCoV-OC43 and HCoV-NL63. HCT-8 and LLC-MK2 were infected with HCoV-OC43 (A) or HCoV-NL63 (B) at a MOI of 0.1 and 0.01, respectively, and treated with serial dilutions of **I-13e** and remdesivir 1 h post infection. The impact of treatment on cell viability was measured by MTS assay after 120 h post infection. Results shown are the average of three independent experiment, and error bars indicate SD.

coronavirus strains at a multiplicity of infection (MOI) of 0.1 and 0.01, respectively, and then treated the cells with serial dilutions of **I-13e**. As shown in Figure 8, **I-13e** exhibited a dose-dependent inhibitory effect on the replication of both viruses. The result showed EC_{50} values of 1.3 and >25 μM for **I-13e** against HCoV-OC43 and HCoV-NL63, respectively, suggesting that **I-13e** is able to inhibit both viruses but exhibits better potency against HCoV-OC43 compared with HCoV-NL63.

DISCUSSION

Many compounds such as ribavirin, favipiravir, and penciclovir were shown to have inhibitory activity toward SARS-CoV-2 RdRp in vitro or in computer-aided molecular modeling studies.[30,31] Most of these inhibitors are NAs, and the structures of these compounds are similar enough to nucleotides to be incorporated into growing viral RNA strands or act as chain terminators to stop the viral RNA synthesis. However, developing NAs as anti-SARS-CoV-2 drugs is challenging for the exonuclease (ExoN) activity encoded by the viral nsp14 protein, which can excise erroneous mutagenic nucleotides incorporated by nsp12 into viral RNA, thus creating resistance to many NAs,[29,32] such as ribavirin. In this situation, non-nucleoside inhibitors (NNIs) of RdRp may be another alternative to be considered.

In this study, we found that quinoline derivatives **I-13e**, **I-13h**, and **I-13i** exhibit remarkable potency in inhibiting RNA synthesis by SARS-CoV-2 RdRp. Based on the activity, the change of the C-2 group of quinoline increased the activity significantly, indicating that the following work should focus on the modification at C-2 by introducing some large hydrophobic/hydrophilic groups. However, quinazoline derivatives displayed moderate to low activity, which requires us to do more work to explore their structure−activity relationships. Among these three compounds, **I-13e** showed the strongest inhibition upon RNA synthesis by SARS-CoV-2 RdRp and the resistance to viral exoribonuclease activity, as well as potent activity against the replication of CoV, thus holding the potential of being a drug candidate for the treatment of SARS-CoV-2.

METHODS

Cell Lines and Viruses. HEK293T, HCT-8, and LLC-MK2 cells were obtained from American Type Culture Collection (ATCC) and cultured in Dulbecco's modified Eagle's medium (DMEM; Gibco, Thermo Fisher Scientific, Waltham, MA, USA) with 10% (v/v) fetal bovine serum (FBS; Gibco) and incubated at 37 °C in a humidified atmosphere of 5% CO_2. HEK293T cells were transfected using Vigofect transfection reagents (Vigorous), according to the manufacturer's instructions.

HCoV-OC43 (VR-1558) was used to infect monolayers of HCT-8 cells at a MOI of 0.1. The HCoV-NL63 strain Amsterdam I was used to infect monolayers of LLC-MK2 cells a MOI of 0.01.

Plasmid DNA and Compounds. The plasmids pCOVID19 nsp12, pCOVID19 nsp7, pCOVID19 nsp8, pCOVID19 nsp10, and pCOVID19 nsp14 were used for codon-optimized Flag-nsp12, Flag-nsp7, Flag-nsp8, Flag-nsp10, and Flag-nsp14, respectively, all of which contain a Flag tag at the C-terminus. pCoV-Gluc producing positive-strand vRNA encoding Gaussia luciferase (Gluc) was under a tetracycline regulated expression promoter and flanked by 5′ and 3′ untranslated regions (UTRs) of SARS-COV-2.

All the quinoline and quinazoline derivatives described herein have been published. For experimental details and compound characterization, please refer to the literature.[18,23,24] The concrete synthetic procedures, the physical characteristics, and NMR for all the compounds are also listed in the Supporting Information. Remdesivir (S8932) and penciclovir (S4184) were purchased from Selleck chemicals (Houston, TX, USA) and prepared in DMSO. Compounds were judged to be at least 95% pure as analyzed by HPLC.

Real-Time RNA Isolation and Quantitative RT-PCR. Cells were cultured with DMEM with 10% FBS for 24 h before treatment with 5 or 10 μM remdesivir or test compounds for 24 h. Total RNA was extracted with TRIzol reagent (Life Technologies) according to the manufacturer's instructions. cDNA was synthesized using primer plus-Gluc-RT (5′-TGG ATC TTG CTG GCG AAT GT-3′) or minus-Gluc- RT (5′-ACT GTC GTT GAC AGG ACA CG-3′) for 1 h at 37 °C. The cDNAs were quantified using SsoFast EvaGreen Supermix (Bio-Rad) in an applied system (Thermo Fisher Scientific). Primers used for PCR are Gluc forward (5′-CGG GTG TGA CCG AAA GGT AA-3′) and reverse (5′-TGG ATC TTG CTG GCG AAT GT-3′). The mRNA expression levels were normalized to GAPDH using primers forward (5′-GTC CAC

https://doi.org/10.1021/acsinfecdis.1c00083
ACS Infect. Dis. 2021, 7, 1535−1544

TGG CGT CTT CAC CA-3′) and reverse (5′-GTG GCA GTG ATG GCA TGG AC-3′).

Cell Viability Assay. The cell viability of compounds on HEK293T cells was evaluated by using the Cell Counting kit-8 (CCK8, Beyotime), which is a water-soluble tetrazolium salt-8 (WST-8) reagent. Briefly, 1 μL of each tested compound ranging from 0.78 to 100 μM was added to cells and incubated for 24 h. Then 10 μL of CCk-8 reagent was added into each well and incubated for 30 to 90 min at 37 °C of 5% CO_2. The absorbance at 450 nm was measured using the Enspire 2300 Multiable reader (PekinElmer).

Gluc Activity Assay. A stock of coelenterazine-h (Promega) was dissolved in absolute ethyl alcohol to a concentration of 1.022 mmol/L. Briefly, the stock was diluted in PBS to 16.7 μM and incubated in the dark for 30 min at room temperature. For the luminescence assay, 10 μL of culture supernatant was added to each well of a white and opaque 96-well plate and mixed with 60 μL of 16.7 μM coelenterazine-h. The luminescence was acquired for 0.5 s using the Berthold Centro XS3 LB 960 microplate luminometer.

Biolayer Interferometry (BLI) Binding Assay. All binding affinity and kinetic profiles were conducted using a ForteBio Octet RED96 instrument (ForteBio, Inc., CA, USA) equipped with super streptavidin biosensor chips (ForteBio). Purified His-tagged nsp12 (50 μg/mL) were captured via Ni-NTA biosensors (960 s, at 25 °C, with 1000 rpm). Ligand biosensors and reference biosensors were dipped into multiple concentrations of test compounds for 60 s (k_{on},1/Ms) then dissociation occurred for 60 s (k_{dis}, 1/s). Blank binding using buffer was used to correct the baseline shift during the analysis. Data analysis on the ForteBio Octet RED instrument was performed using a reference well subtraction in the ForteBio data analysis software.

Anticoronavirus Activity Assay. The anticoronavirus activity of the different strains was measured by using MTS Cell Proliferation Colorimetric assay kits (Promega, Madison, WI, USA). Briefly, HCT-8 cells and LLC-MK2 cells were inoculated with HCoV-OC43 and HCoV-NL63 at a MOI of 0.1 and 0.01 respectively, containing 2% FBS and each of test compounds. Cells were then incubated at 33 °C for 120 h in a 5% CO_2 incubator. Then 20 μL of MTS Cell Proliferation Colorimetric reagent was added into each well and incubated for 3 h at 37 °C in 5% CO_2. The absorbance at 490 nm was measured using the Enspire 2300 Multiable reader (PekinElmer).

Statistical Analysis. Data are presented as the means ± SD from at least three independent experiments. Data were analyzed with GraphPad Prism. Differences between groups were considered statistically significant if $p < 0.01$(**) and $p < 0.001$(***), and NS represents not significant.

■ ASSOCIATED CONTENT

Supporting Information

The Supporting Information is available free of charge at https://pubs.acs.org/doi/10.1021/acsinfecdis.1c00083.

Structure−activity relationship analysis of 101 quinoline and quinazoline upon RNA synthesis by SARS-CoV-2 RdRp; experimental and NMR spectra data for quinoline and quinazoline derivatives; effects of compounds **I-13e**, **I-13h**, and **I-13i** on Gluc plasmid mRNA level; HPLC-MS spectra of compound **I-13e** in DMEM at 37 °C for 24 h (PDF)

■ AUTHOR INFORMATION

Corresponding Authors

Xiaoyu Li − *Institute of Medicinal Biotechnology, Chinese Academy of Medical Science, Beijing 100050, China*; Email: lixiaoyu@imb.pumc.edu.cn

Yucheng Wang − *Institute of Medicinal Biotechnology, Chinese Academy of Medical Science, Beijing 100050, China*; Email: wangyucheng@imb.pumc.edu.cn

Shan Cen − *Institute of Medicinal Biotechnology, Chinese Academy of Medical Science, Beijing 100050, China*; orcid.org/0000-0003-3358-0411; Email: shancen@imb.pumc.edu.cn

Authors

Jianyuan Zhao − *Institute of Medicinal Biotechnology, Chinese Academy of Medical Science, Beijing 100050, China*

Yongxin Zhang − *Institute of Medicinal Biotechnology, Chinese Academy of Medical Science, Beijing 100050, China*

Minghua Wang − *Institute of Medicinal Biotechnology, Chinese Academy of Medical Science, Beijing 100050, China*

Qian Liu − *Institute of Medicinal Biotechnology, Chinese Academy of Medical Science, Beijing 100050, China*

Xiaobo Lei − *Institute of Pathogen Biology, Chinese Academy of Medical Science, Beijing 100730, China*

Meng Wu − *Department of Urology, Beijing Hospital, Beijing 100730, China*

SaiSai Guo − *Institute of Medicinal Biotechnology, Chinese Academy of Medical Science, Beijing 100050, China*

Dongrong Yi − *Institute of Medicinal Biotechnology, Chinese Academy of Medical Science, Beijing 100050, China*

Quanjie Li − *Institute of Medicinal Biotechnology, Chinese Academy of Medical Science, Beijing 100050, China*

Ling Ma − *Institute of Medicinal Biotechnology, Chinese Academy of Medical Science, Beijing 100050, China*

Zhenlong Liu − *Lady Davis Institute for Medical Research and McGill AIDS Centre, Jewish General Hospital, Montreal, Quebec H3T 1E2, Canada*

Fei Guo − *Institute of Pathogen Biology, Chinese Academy of Medical Science, Beijing 100730, China*

Jianwei Wang − *Institute of Pathogen Biology, Chinese Academy of Medical Science, Beijing 100730, China*

Complete contact information is available at: https://pubs.acs.org/10.1021/acsinfecdis.1c00083

Author Contributions

⊥J.Z., Y.Z., M.W., and Q.L. contributed equally to this work.

Notes

The authors declare no competing financial interest.

■ ACKNOWLEDGMENTS

This work was supported by The National Mega-Project for Infectious Disease (2018ZX10301408), The National Mega-Project for Significant New Drug Discovery (2018ZX09711003-002-002), The National Key Research and Development program of China (2018YFE0107600 and 2016YFD0500307), CAMS Innovation Fund for Medical Sciences (2018-I2M-3-004 and 2020-12M-2-010), and the Fundamental Research Funds for the Central Universities (33320200046). We thank National Infrastructure of Micro-

bial Resources (NIMR-2014-3) and CAMS Collection Center of Pathogenic Micro-organisms (CAMS-CCPM-A) for providing valuable reagents.

REFERENCES

(1) Chen, N., Zhou, M., Dong, X., Qu, J., Gong, F., Han, Y., Qiu, Y., Wang, J., Liu, Y., Wei, Y., Xia, J., Yu, T., Zhang, X., and Zhang, L. (2020) Epidemiological and clinical characteristics of 99 cases of 2019 novel coronavirus pneumonia in Wuhan, China: a descriptive study. *Lancet 395* (10223), 507−513.

(2) Wu, Z., and McGoogan, J. M. (2020) Characteristics of and Important Lessons From the Coronavirus Disease 2019 (COVID-19) Outbreak in China: Summary of a Report of 72 314 Cases From the Chinese Center for Disease Control and Prevention. *JAMA 323* (13), 1239−1242.

(3) Chen, T., Wu, D., Chen, H., Yan, W., Yang, D., Chen, G., Ma, K., Xu, D., Yu, H., Wang, H., Wang, T., Guo, W., Chen, J., Ding, C., Zhang, X., Huang, J., Han, M., Li, S., Luo, X., Zhao, J., and Ning, Q. (2020) Clinical characteristics of 113 deceased patients with coronavirus disease 2019: retrospective study. *BMJ. 368*, m1091.

(4) WHO. Coronavirus Disease 2019 (COVID-19) Situation Report, April 18, 2021.

(5) Hu, B., Ge, X., Wang, L., and Shi, Z. (2015) Bat origin of human coronaviruses. *Virol. J. 12*, 221.

(6) Li, W., Shi, Z., Yu, M., Ren, W., Smith, C., Epstein, J. H., Wang, H., Crameri, G., Hu, Z., Zhang, H., Zhang, J., McEachern, J., Field, H., Daszak, P., Eaton, B. T., Zhang, S., and Wang, L. (2005) Bats are natural reservoirs of SARS-like coronaviruses. *Science 310* (5748), 676−679.

(7) V'kovski, P., Kratzel, A., Steiner, S., Stalder, H., and Thiel, V. (2021) Coronavirus biology and replication: implications for SARS-CoV-2. *Nat. Rev. Microbiol. 19* (3), 155−170.

(8) Zhou, P., Yang, X., Wang, X., Hu, B., Zhang, L., Zhang, W., Si, H., Zhu, Y., Li, B., Huang, C., Chen, H., Chen, J., Luo, Y., Guo, H., Jiang, R., Liu, M., Chen, Y., Shen, X., Wang, X., Zheng, X., Zhao, K., Chen, Q., Deng, F., Liu, L., Yan, B., Zhan, F., Wang, Y., Xiao, G., and Shi, Z. (2020) A pneumonia outbreak associated with a new coronavirus of probable bat origin. *Nature 579* (7798), 270−273.

(9) Wu, F., Zhao, S., Yu, B., Chen, Y., Wang, W., Song, Z., Hu, Y., Tao, Z., Tian, J., Pei, Y., Yuan, M., Zhang, Y., Dai, F., Liu, Y., Wang, Q., Zheng, J., Xu, L., Holmes, E., and Zhang, Y. (2020) A new coronavirus associated with human respiratory disease in China. *Nature 579* (7798), 265−269.

(10) Gao, Y., Yan, L., Huang, Y., Liu, F., Zhao, Y., Cao, L., Wang, T., Sun, Q., Ming, Z., Zhang, L., Ge, J., Zheng, L., Zhang, Y., Wang, H., Zhu, Y., Zhu, C., Hu, T., Hua, T., Zhang, B., Yang, X., Li, J., Yang, H., Liu, Z., Xu, W., Gullat, L. W., Wang, Q., Lao, Z., and Rao, Z. (2020) Structure of the RNA-dependent RNA polymerase from COVID-19 virus. *Science 368* (6492), 779−782.

(11) Tvarogová, J., Madhugiri, R., Bylapudi, G., Ferguson, L. J., Karl, N., and Ziebuhr, J. (2019) Identification and Characterization of a Human Coronavirus 229E Nonstructural Protein 8-Associated RNA 3′-Terminal Adenylyltransferase Activity. *J. Virol. 93* (12), e00291-19.

(12) Hillen, H. S., Kokic, G., Farnung, L., Dienemann, C., Tegunov, D., and Cramer, P. (2020) Structure of replicating SARS-CoV-2 polymerase. *Nature 584* (7819), 154−156.

(13) Nanda, A. K., Ganguli, S., and Chakraborty, R. (2007) Antibacterial activity of some 3-(arylideneamino)-2-phenylquinazoline-4(3H)-ones: synthesis and preliminary QSAR studies. *Molecules 12* (10), 2413−2426.

(14) Xu, G., Song, B., Bhadury, P. S., Yang, S., Zhang, P., Jin, L., Xue, W., Hu, D., and Lu, P. (2007) Synthesis and antifungal activity of novel s-substituted 6-fluoro-4-alkyl(aryl)thioquinazoline derivatives. *Bioorg. Med. Chem. 15* (11), 3768−3774.

(15) Lv, Y., Wang, X., Song, B., Yang, S., Yan, K., Xu, G., Bhadury, P. S., Liu, F., Jin, L., and Hu, D. (2007) Synthesis, antiviral and antifungal bioactivity of 2-cyano-acrylate derivatives containing phosphonyl moieties. *Molecules 12* (5), 965−978.

(16) Yang, S., Li, Z., Jin, L., Song, B., Liu, G., Chen, J., Chen, Z., Hu, D., Xue, W., and Xu, R. (2007) Synthesis and bioactivity of 4-alkyl(aryl)thioquinazoline derivatives. *Bioorg. Med. Chem. Lett. 17* (8), 2193−2196.

(17) Wan, Z., Hu, D., Li, P., Xie, D., and Gan, X. (2015) Synthesis, Antiviral Bioactivity of Novel 4-Thioquinazoline Derivatives Containing Chalcone Moiety. *Molecules 20* (7), 11861−11874.

(18) Zhang, G., Wang, M., Zhao, J., Wang, Y., Zhu, M., Wang, J., Cen, S., and Wang, Y. (2020) Design, synthesis and in vitro anti-influenza A virus evaluation of novel quinazoline derivatives containing S-acetamide and NH-acetamide moieties at C-4. *Eur. J. Med. Chem. 206*, 112706.

(19) Zheng, X., Liang, C., Wang, L., Wang, B., Liu, Y., Feng, S., Wu, J. Z., Gao, L., Feng, L., Chen, L., Guo, T., Shen, H. C., and Yun, H. (2018) Discovery of Benzoazepinequinoline (BAQ) Derivatives as Novel, Potent, Orally Bioavailable Respiratory Syncytial Virus Fusion Inhibitors. *J. Med. Chem. 61* (22), 10228−10241.

(20) Sharma, A., Slaughter, A., Jena, N., Feng, L., Kessl, J. J., Fadel, H. J., Malani, N., Male, F., Wu, L., Poeschla, E., Bushman, F. D., Fuchs, J. R., and Kvaratskhelia, M. (2014) A new class of multimerization selective inhibitors of HIV-1 integrase. *PLoS Pathog. 10* (5), e1004171.

(21) Cui, Q., Cheng, H., Xiong, R., Zhang, G., Du, R., Anantpadma, M., Davey, R. A., and Rong, L. (2018) Identification of Diaryl-Quinoline Compounds as Entry Inhibitors of Ebola Virus. *Viruses 10* (12), 678.

(22) Carta, A., Briguglio, I., Piras, S., Corona, P., Boatto, G., Nieddu, M., Giunchedi, P., Marongiu, M. E., Giliberti, G., Iuliano, F., Blois, S., Ibba, C., Busonera, B., and La Colla, P. (2011) Quinoline tricyclic derivatives. Design, synthesis and evaluation of the antiviral activity of three new classes of RNA-dependent RNA polymerase inhibitors. *Bioorg. Med. Chem. 19* (23), 7070−7084.

(23) Wang, M., Zhang, G., Wang, Y., Wang, J., Zhu, M., Cen, S., and Wang, Y. (2020) Design, synthesis and anti-influenza A virus activity of novel 2,4-disubstituted quinazoline derivatives. *Bioorg. Med. Chem. Lett. 30* (11), 127143.

(24) Wang, M., Zhang, G., Zhao, J., Cheng, N., Wang, Y., Fu, Y., Zheng, Y., Wang, J., Zhu, M., Cen, S., He, J., and Wang, Y. (2021) Synthesis and antiviral activity of a series of novel quinoline derivatives as anti-RSV or anti-IAV agents. *Eur. J. Med. Chem. 214*, 113208.

(25) Wentland, M. P., Perni, R. B., Dorff, P. H., Brundage, R. P., Castaldi, M. J., Carlson, J. A., Bailey, T. R., Aldous, S. C., Carabateas, P. M., Bacon, E. R., Kullnig, R. K., Young, D. C., Woods, M. G., Kingsley, S. D., Ryan, K. A., Rosi, D., Drozd, M. L., and Dutko, F. J. (1997) Antiviral properties of 3-quinolinecarboxamides: a series of novel non-nucleoside antiherpetic agents. *Drug Des. Discovery 15* (1), 25−38.

(26) Guo, R., Zhang, Q., Ma, Y., Huang, X., Luo, J., Wang, L., Geng, C., Zhang, X., Zhou, J., Jiang, Z., and Chen, J. (2011) Synthesis and biological assay of 4-aryl-6-chloro-quinoline derivatives as novel non-nucleoside anti-HBV agents. *Bioorg. Med. Chem. 19* (4), 1400−1408.

(27) Zhao, J., Guo, S., Yi, D., Li, Q., Ma, L., Zhang, Y., Wang, J., Li, X., Guo, F., Lin, R., Liang, C., Liu, Z., and Cen, S. (2021) A cell-based assay to discover inhibitors of SARS-CoV-2 RNA dependent RNA polymerase. *Antiviral Res. 190*, 105078.

(28) Yin, W., Mao, C., Luan, X., Shen, D., Shen, Q., Su, H., Wang, X., Zhou, F., Zhao, W., Gao, M., Chang, S., Xie, Y., Tian, G., Jiang, H., Tao, S., Shen, J., Jiang, Y., Jiang, H., Xu, Y., Zhang, S., Zhang, Y., and Xu, H. (2020) Structural basis for inhibition of the RNA-dependent RNA polymerase from SARS-CoV-2 by remdesivir. *Science 368* (6498), 1499−1504.

(29) Ma, Y., Wu, L., Shaw, N., Gao, Y., Wang, J., Sun, Y., Lou, Z., Yan, L., Zhang, R., and Rao, Z. (2015) Structural basis and functional analysis of the SARS coronavirus nsp14-nsp10 complex. *Proc. Natl. Acad. Sci. U. S. A. 112* (30), 9436−9441.

(30) Faheem, Kumar, B. K., Sekhar, K., Kunjiappan, S., Jamalis, J., Balaña-Fouce, R., Tekwani, B. L., and Sankaranarayanan, M. (2020)

https://doi.org/10.1021/acsinfecdis.1c00083
ACS Infect. Dis. 2021, 7, 1535−1544

Druggable targets of SARS-CoV-2 and treatment opportunities for COVID-19. *Bioorg. Chem. 104*, 104269.
(31) Elfiky, A. A. (2020) Ribavirin, Remdesivir, Sofosbuvir, Galidesivir, and Tenofovir against SARS-CoV-2 RNA dependent RNA polymerase (RdRp): A molecular docking study. *Life Sci. 253*, 117592.
(32) Ferron, F., Subissi, L., Silveira De Morais, A. T., Le, N., Sevajol, M., Gluais, L., Decroly, E., Vonrhein, C., Bricogne, G., Canard, B., and Imbert, I. (2018) Structural and molecular basis of mismatch correction and ribavirin excision from coronavirus RNA. *Proc. Natl. Acad. Sci. U. S. A. 115* (2), E162−E171.

https://doi.org/10.1021/acsinfecdis.1c00083
ACS Infect. Dis. 2021, 7, 1535−1544